

Mesh Sensitivity and FEA for Multi-Layered Electronic Packaging

Cemal Basaran

Assoc. Prof. and Director,
UB Electronic Packaging Laboratory,
University at Buffalo, SUNY,
Buffalo, NY 14260
e-mail: cjb@eng.buffalo.edu

Ying Zhao

Senior Reliability Engineer,
Analog Devices,
Norwood, MA

Multi-layered stacks are commonly used in microelectronic packaging. Traditionally, these systems are designed using linear-elastic analysis either with analytical solutions or finite element method. Linear-elastic analysis for layered structures yields very conservative results due to stress singularity at the free edge. In this paper, it is shown that a damage mechanics based nonlinear analysis not just leads to a more realistic analysis but also provides more accurate stress distribution. In this paper these two approaches are compared. Moreover, mesh sensitivity of the finite element analysis in stack problems is studied. It is shown that the closed form and elastic finite element analyses can only be used for preliminary studies and elastic finite element method is highly mesh sensitive for this problem. In elastic analysis the stress singularity at the free edge makes mesh selection very difficult. Even when asymptotic analysis is used at the free edge, the results are very conservative compared to an inelastic analysis. Rate sensitive inelastic analysis does not suffer from the stress singularity and mesh sensitivity problems encountered in elastic analysis. [DOI: 10.1115/1.1362674]

Introduction

A number of researchers proposed closed-form solutions for stresses in laminated stacks subjected to temperature gradient. These closed-form equations offer a rapid method to obtain stresses in the materials and the interfaces. Hence, in the microelectronics industry it is very common to use elastic analysis to analyze and design these laminated stacks.

Delamination of the interfaces and shear fatigue of the adhesive material are the critical failure modes for these structures.

Comparisons between the elastic and the inelastic results are presented to demonstrate that elastic analysis significantly overestimates the maximum shear stress because of stress singularity near the free edge. Finite element analysis is often used to prove the accuracy of closed-form solutions, Chen et al. [1], Glaser [2], Jiang et al. [3] and many others. In this study, it is shown that, there is a significant difference between the FEA results obtained from different meshes and closed-form solutions. It is also shown that for design and reliability analysis thermo-viscoplastic analysis is a more accurate procedure. Experimental results for a layered package are also presented to show that elastic analysis is too conservative.

Bi-metal thermostat beam theory was first addressed by Timoshenko [4]. Thermal stresses in multilayered beams and plates has also been studied by Boley and Testa [5], Wang and Crossmann [6], Grimado [7], Wang and Choi [8], Chen et al. [1], Chang [9], Saganuma et al. [10], Blech and Kantor [11], and Kuo [12], Reddy and Miravete [13], Hutchinson [14] and others. In recent years thermal stresses in multilayered assemblies have received a significant amount of attention in the field of electronic packaging. Thermal stresses in bonded joints within microelectronics devices were first studied by Dash [15]. A number of papers proposed various approximate methods to predict the free-edge interlaminar stresses introduced by thermal and mechanical loads. Some of the papers published on this subject are—Taylor and Yuan [16], Bogy [17,18], Hein and Erdogan [19], Zeyfang [20], Reinhart and Logan [21], Roll [22], Olsen and Ettenberg [23], Vilms and Kerps [24], Chen et al. [1], Glascock and Webster

[25], Suhir [26–31,42,43] and Gerstle and Chambers [32], Glaser [2], Yin [33], Pao and Eisele [34], Morgan [35], Jiang et al. [3] and others.

Most of the proposed methods are aimed at the evaluation of stresses in the layers themselves and therefore can be used only for an indirect judgment of the level of interfacial stresses where delamination and peeling takes places.

Suhir [28–31] proposed an analytical procedure, widely known as the Suhir solution, for predicting the magnitude and the distribution of thermal stresses in single and multilayered heteroepitaxial structures. The Suhir solution is the most commonly used benchmark analytical procedure in the electronic packaging literature. He suggested a theoretical model taking into account the elastoplastic behavior of the attachment material and, in particular, of solder interconnections. Suhir introduced a concept of longitudinal and transverse interfacial compliance and combined them into an engineering approach to estimate the thermal stresses in two-layered bonded finite joints. Later Suhir extended his approach to multilayered thin stacks by making certain assumption on the compatibility condition of the interface and introduced an interface compliance. Pao and Eisele [34] extended Suhir's elastic bimetal model to multilayered thin stacks without imposing any additional assumptions on the interface.

The main drawback of analytical solutions is that they cannot be used for analysis of structures with irregular geometry, non-smooth boundaries, and varying material properties. The stress equilibrium in the direction normal to the layers is not satisfied unless an additional concentrated force is introduced at the free edge.

It has been shown by Bogy [17,18], Hein and Erdogan [19], Yin [33] and others that an exact analysis with strict adherence to the constitutive relations of linear elasticity yields a stress singularity at the intersection of the free edge with an interface. Such a stress singularity cannot be directly determined by the standard elastic finite element analysis alone. Asymptotic analysis is needed to determine the stresses in the near-tip stress field, Lee and Jasiuk [36]. In real life, this stress singularity does not exist. Once the stress level reaches the yield strength of the material it yields and stress is redistributed to neighboring points. Therefore using an inelastic constitutive model better simulates the actual phenomenon that takes place in the material.

In this study we show that the elastic FEA results are strongly

Contributed by the Electrical and Electronic Packaging Division for publication in the JOURNAL OF ELECTRONIC PACKAGING. Manuscript received by the EEPD July 6, 1999. Associate Editor: B. Michel.

mesh sensitive, in particular, near the free edge where there is stress singularity. Since the adhesive layer is designed for the maximum stresses at the free edge, maximum values obtained from the analysis are critical.

It should be pointed out that the mesh sensitivity discussed here is not the monotonic convergence of FEA results by mesh refinement. It is very well known that in a monotonically converging FEA as the mesh is refined the results converge to the exact solution of the partial differential equation. The mesh sensitivity encountered in bimaterial structures is due to the stress singularity near the free edge. As the element size near the free edge gets smaller the singularity is localized and stress level in that element increases.

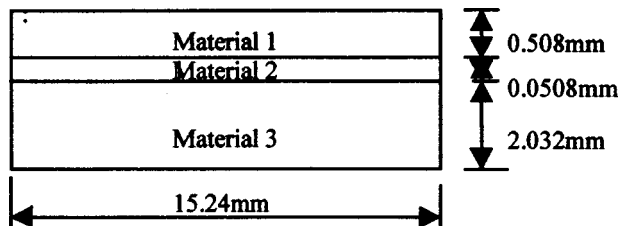
It is well known that most commonly used bonding material in microelectronics industry is Pb/Sn solder. This material operates at high homologous temperatures due to its low melting point 183°C. The dominant failure mode for Pb40/Sn60 material under thermal cycling is creep-damage, Basaran [37], Zhao et al. [38]. Hence, special attention is paid to the viscoplastic behavior exhibited by the adhesive solder material. Therefore the closed-form solutions proposed in the literature can only be used to get a preliminary estimate of stresses and strain in the adherent layers but not the adhesive layer or the interfaces.

Elastic Analysis

The purpose of this section is to show that elastic FEA is mesh sensitive for laminated structures mainly due to stress singularity. ABAQUS elastic analysis results are compared with Suhir solution.

Three meshes with significantly different refinement levels are used to exhibit mesh-sensitivity of this problem. One is relatively fine mesh with 1380 elements, one is very fine mesh with 6440 elements, and one is extremely fine mesh with 9900 elements. The smallest element dimension in the finest mesh (25 μm) is at the same order as single Pb/Sn solder grain diameter, (usually between 5 μm to 25 μm). The structure is modeled with 8 node plane strain elements. The geometry and material properties of the model, Fig. 1, are taken from Glaser [2] for comparison purposes.

The adhesive layer shear stress distributions along the interface are shown in Fig. 2(a)–Fig. 2(c) for three different mesh refinement cases. Significant discrepancy occurs among the FEA results, as well as between the FEA results and that of the Suhir solution. Even though the results are qualitatively comparable, they are quantitatively quite different. For the first case, the maximum shear stress in the adhesive layer is 77 MPa, compared with 95 MPa for the second case and 103 MPa for the third case, a 34 percent difference between mesh 1 and mesh 3. In Suhir's closed-form solution there is no singularity close to the edge, and the maximum value 115 Mpa occurs at the point of the free edge. The difference between the maximum value from the Suhir solution and the finest mesh is 11 percent and the difference between the



Material 1	Material 2	Material 3
E=68.95 GPa	E=13.0GPa	E=120.66GPa
ν=0.33	ν=0.3	ν=0.28
α=23.6E-6/°C	α=11.7E-6/°C	α=3.2E-6/°C

Fig. 1 Geometry and material properties

coarsest mesh and the Suhir solution is 49 percent. This difference proves that elastic FEM with standard formulation cannot be used to judge quantitative accuracy of analytical solutions.

The adhesive layer transverse normal (peeling) stress distribution is shown in Fig. 3(a)–Fig. 3(c) for three different meshes. The stresses shown in the figures are Gauss point average element stresses. In finite element analysis results there is a peak in the negative area as well as a sharp peak near the free edge for all

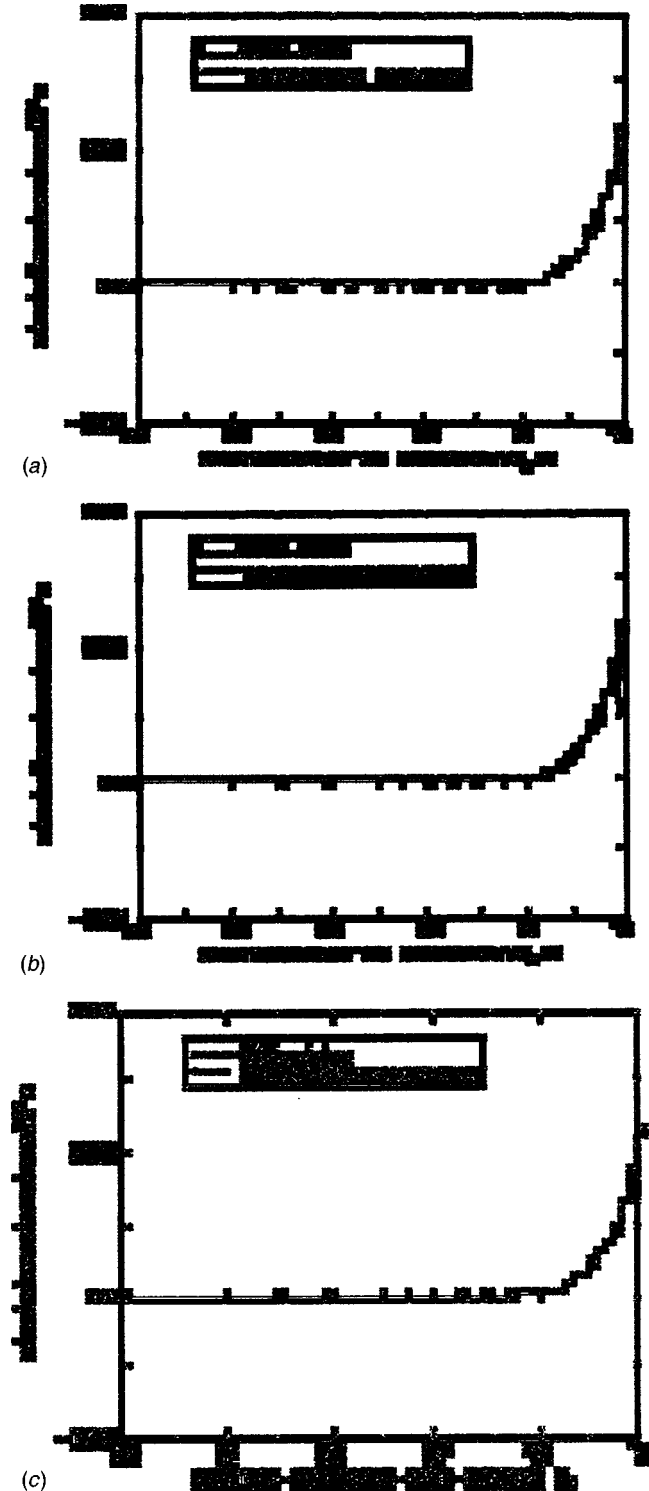


Fig. 2 (a) Elastic FEA with 1380 elements. (b) Elastic FEA with 6440 elements. (c) Elastic FEA with 9900 elements.

refinement levels. The peeling stress also drops dramatically near the free edge except for the coarse mesh. The stress drop near the free edge is due to the stress free boundary condition. The coarse mesh cannot capture this drop due to the stress singularity and the very low stress values are in the same element. In the first case, the peak value is 25.5 MPa, while the minimum is -23.3 MPa. In the second case, they are 46 MPa and -12.3 MPa, and in the third

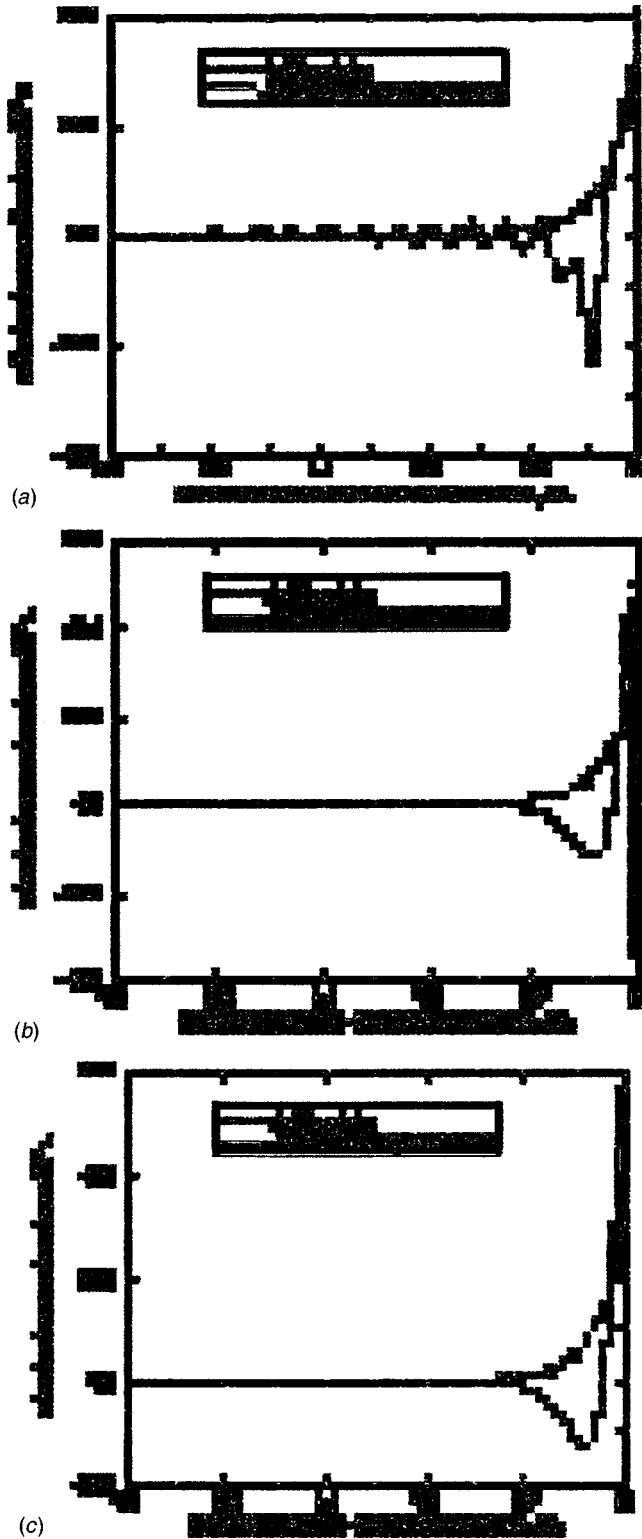


Fig. 3 (a) Elastic FEA with 1380 elements. (b) Elastic FEA with 6440 elements. (c) Elastic FEA with 9900 elements.

case they are 57.2 MPa and -12.4 MPa. The transverse normal stress distribution calculated from Suhir's equation yields a maximum value of about 40 MPa, and there is no compression zone. The difference between the Suhir solution and the courses mesh and finest mesh is 56 percent and 30 percent, respectively.

Both FEA and closed-form solution yield high shear and peeling stresses near the free edge and almost no stresses in most of the inner part of the interface. This type of stress distribution does not agree well with our experimental observations discussed later in the paper. Actual stress distribution does not have extreme stress gradients; change is smooth and gradual.

Elasto-Viscoplastic Analysis

In this part of the study the thin adhesive layer is modeled with the viscoplastic constitutive model in ABAQUS and the adherent layers as elastic materials.

In viscoplastic analysis, the layered assembly is subjected to a uniform temperature change from 27°C-147°C. The shear and peeling stress distributions are plotted in Figs. 4 and 5. In Elasto-viscoplastic analysis the stresses are spread over a wider zone near the free edge. About 20 percent of the total length is subjected to a relatively uniform shear stress compared to a very narrow region

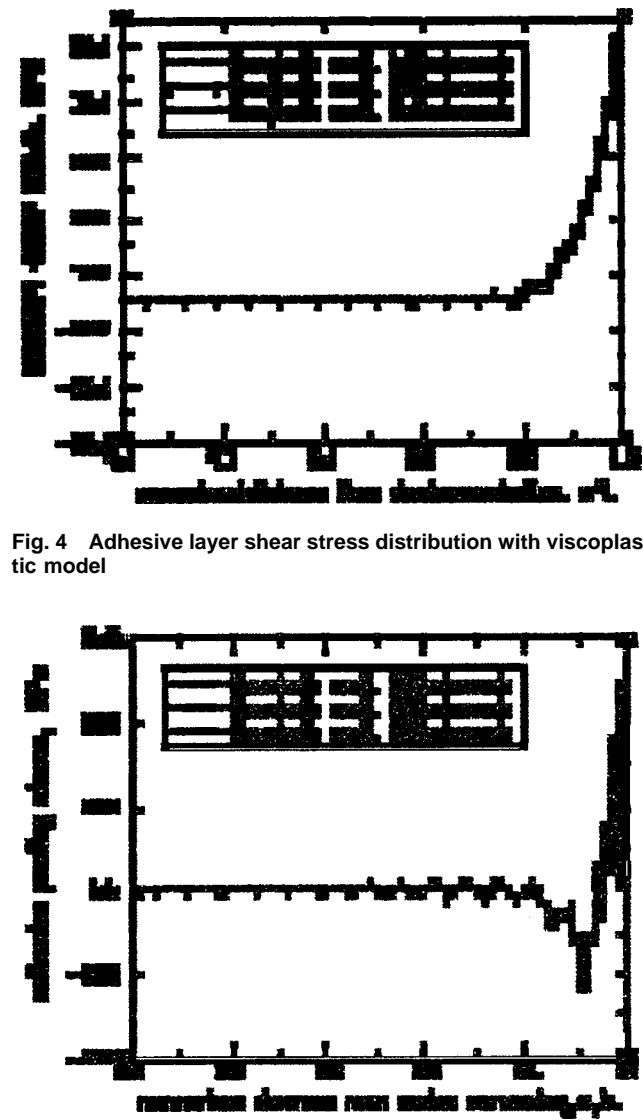


Fig. 4 Adhesive layer shear stress distribution with viscoplastic model

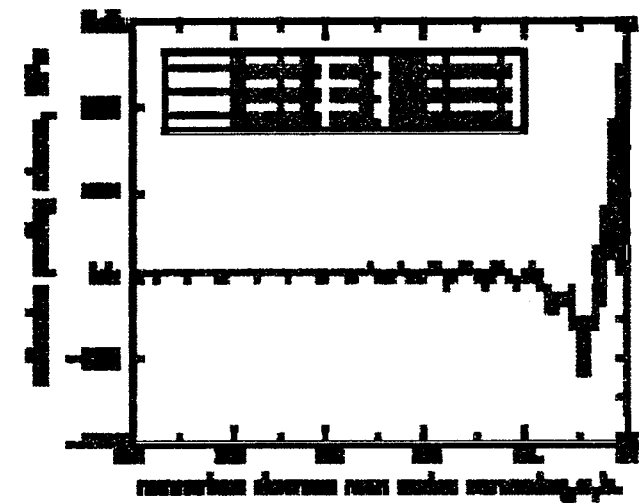


Fig. 5 Adhesive layer peeling stress distribution with viscoplastic model

in elastic analysis. The peeling stress starts to change from zero at the point of 0.64 L, compared to the critical point 0.8 L in the elastic case. This is in spite of the fact that the temperature gradient used in the viscoplastic analysis is much smaller. This indicates that in viscoplastic analysis the stress is actually relaxed and is spread to nearby area by inelastic deformation.

In the three cases of different mesh refinement the stress distributions along the interface are almost the same, except that there is some fluctuation of peeling stress distribution in the case of the coarsest mesh. Compared to elastic analysis, the results are not sensitive to mesh refinement in viscoplastic analysis. The shear stress in adhesive layer is 14.8 for the mesh with 1380 element and 15.0 MPa for the other two meshes. The peeling stress is 5.2 Mpa for the coarsest mesh, 10.4 for the medium, and 10.6 for the finest mesh. Based on this comparison one can say that rate dependent analysis yields significantly less mesh sensitive results for this problem.

Thermo Elasto-Viscoplastic with Damage Analysis

The material model used in this part of the study is based on continuum damage mechanics formulation

$$d\sigma_{ij} = (1 - D)C_{ijkl}d\varepsilon_{kl} \quad (1)$$

where $d\sigma_{ij}$ is the incremental average stress tensor, D is the isotropic accumulated damage, C_{ijkl} is the tangential constitutive tensors, and $d\varepsilon_{ij}$ is the incremental total strain tensor.

Assuming small strain deformations total strain can be given by summation of strain increment tensors,

$$d\varepsilon_{ij} = d\varepsilon_{ij}^e + d\varepsilon_{ij}^\theta + d\varepsilon_{ij}^{vp} \quad (2)$$

where $d\varepsilon_{ij}^e$, $d\varepsilon_{ij}^\theta$, and $d\varepsilon_{ij}^{vp}$ are the elastic, thermal, and viscoplastic strain increments. The elastic and thermal components of strain tensor are easily obtained from the elasticity relations. The viscoplastic component of the strain is obtained by using a creep rate function for the steady-state regime.

A sine hyperbolic creep law is used to simulate the two regimes of creep process, namely, power law creep (glide and climb) and power-law creep breakdown (obstacle controlled glide, cross slip), Hacke et al. [39]. The adopted creep law takes into account grain size of the solder material. This is very important since it is well known that grain size significantly affects the mechanical behavior of two phase solder alloys, Kashyap and Murty [40]

$$\dot{\varepsilon}_{ij}^{vp} = A (\sinh(B\bar{\sigma}_{eff}))^n d^m \exp\left(-\frac{Q}{RT}\right) \frac{fF}{f\sigma_{ij}} \quad (3)$$

where, A , B , m , n are material constants, d is the average grain size, in μm , Q is the apparent creep activation energy, $\bar{\sigma}_{eff}$ is the von Mises equivalent stress in MPa, R is gas constant, T is material temperature, in Kelvin and F is the yield criterion

The yield surface is given by

$$F = \bar{\sigma}_{eff} - R - k_0 \quad (4)$$

where $\bar{\sigma}_{eff}$ is the effective von Mises stress, R is the evolution of the size of yield surface and k_0 is the initial size of the yield surface.

Damage Evolution Function

Traditionally norm of plastic strain has been used to quantify damage. Plastic strain is a path dependent value in a numerical analysis. Different plastic strain values can be obtained for the same state of stress according to the stress path followed. Basaran and Yan [41] have shown that entropy of a system can be used to quantify damage. Using second law of thermodynamics and statistical continuum mechanics the following damage evolution function can be derived, Basaran and Yan [41]

$$D = 1 - \exp\left(-\frac{\Delta e - \Delta \phi}{N_0 k \theta / \bar{m}_s}\right) \quad (5)$$

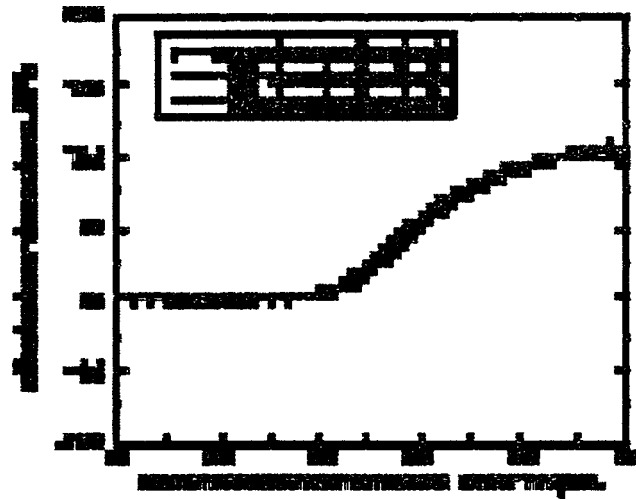


Fig. 6 Adhesive layer shear stress distribution with thermo-elasto-viscoplastic model with damage

$$\Delta e - \Delta \phi = \frac{1}{\rho \varepsilon_0} \sigma_{ij} d\varepsilon_{ij}^p - \frac{1}{\rho t_0} \frac{f q_i}{f X_i} dt + \int_{t_0}^t \dot{\gamma} dt \quad (6)$$

where, N_0 is the Avogadro's number, k is the Boltzmann's constant, θ is the temperature in Kelvin, \bar{m}_s is the specific mass, ρ is unit weight, σ_{ij} is stress tensor, $d\varepsilon_{ij}^p$ is the increment of inelastic strain, q_i is heat flux, and γ_i is the heat production. In this analysis, relatively coarse meshes were used to show that for thermo-elasto-viscoplastic with damage analysis results are not mesh sensitive. Mesh I has 232 elements, mesh II has 390 elements, and mesh III has 416 plane strain 8-noded elements.

Figure 6 and Fig. 7 present the adhesive layer shear stress and adhesive layer peeling stress distribution along the interface.

Closed-form solution calculated from the Suhir solution, elastic FEM results, and thermo-viscoplastic with damage results are plotted on the same figure in Fig. 8 and Fig. 9, for adhesive layer shear stress and peeling stress, respectively. Thermo-viscoplastic with damage model yields much lower stresses near the free edge compared to elastic solutions. In nature when the stress at a point level reaches the yield stress that point transfers some of its load to the neighboring point. As a result, in real life stress values can never exceed yield stress and stress singularity cannot exist.

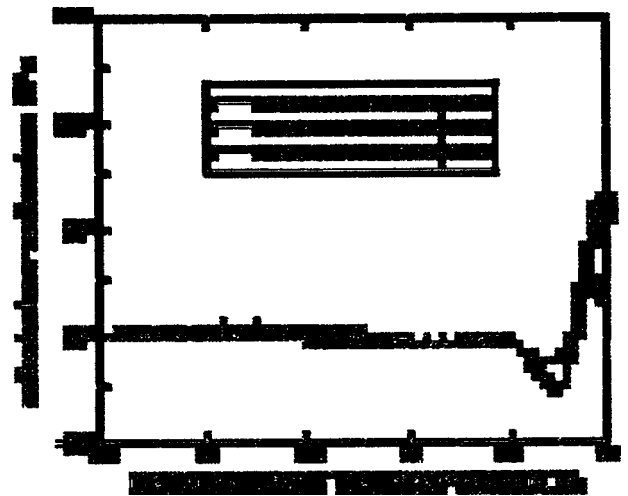


Fig. 7 Adhesive layer peeling stress distribution with thermo-elasto-viscoplastic model with damage

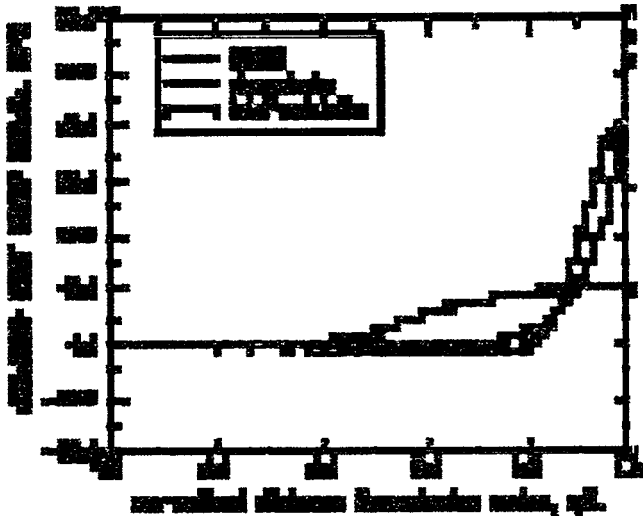


Fig. 8 Adhesive layer shear stress distribution. Comparison between elastic, thermo-elasto-viscoplastic with damage and Suhir solution.

Thermo-viscoplastic with damage model yields a much lower shear stress distributed over a much wider area, compared to a very narrow band of shear stress in elastic analysis. The shear stress is distributed over about 50 percent of the interface compared to 10 percent in elastic analysis. In viscoplastic with damage analysis the shear stress is not mesh sensitive. Figure 7 exhibits some mesh sensitivity albeit significantly less compared to the elastic analysis.

The stress-strain distributions show that when the multilayered structure is under thermal or mechanical loading, shear and peeling stresses and strains are usually built up near the free edge. Shear stress causes the dislocation and plastic sliding to be accumulated, and the peeling stress leads to the tensile failure. Thus it naturally follows that failure will initiate from free edge, and develop toward the inside of the interface.

Near the free edge as the stress exceeds the yield stress the material cannot carry the high stresses and it yields. As a result, high stresses are redistributed to the neighboring points. This redistribution process continues until the system reaches an equilibrium

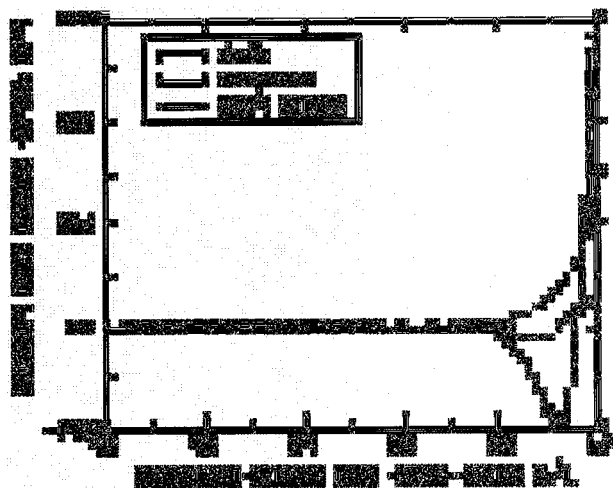


Fig. 9 Adhesive layer peeling stress distribution. Comparison between elastic, thermo-elasto-viscoplastic with damage and Suhir solution.

rium state on the yield surface. Hence, viscoplastic analysis yields a much smoother shear stress distribution with a small gradient compared to elastic analysis.

In elastic analysis, the sharp peak near the free edge is dramatic, indicating some deviation from real material response. In viscoplastic analysis, however, the change in the value of stresses toward the edge is much smoother, which indicates the development of inelastic deformation and stress redistribution along the interface.

Comparison With Experimental Analysis

A Ball Grid Array (BGA) package was tested in thermal cycling and plastic strain field was measured by high sensitivity Moire interferometry. The specimen cross section is shown in Fig. 10. It has a multilayered structure, with three major layers connected by two layers of BGA solder joints. All the solder joints are Sn63/Pb37 eutectic solder alloy. The solder joints of interest are at the bottom layer which bonds two layers with significantly different coefficients of thermal expansion (CTE)—the FR4 layer and the long chain directional polymer layer. These solder joints have been observed to be the most vulnerable interconnections of the entire device. The CTE of the polymer is about 5 orders bigger than the FR4. There are tiny thin copper metallization layers inserted in the polymer, which actually bond to the solder joints.

The specimen was thermally cycled in a high capacity Super AGREE environmental chamber between -55°C and 125°C . The temperature changing rate was $20^{\circ}\text{C}/\text{min}$, the holding time at each extreme end was 12 min, and the period of one cycle was 42 min. The temperature history is shown in Fig. 11. Before cycling, the specimen was used to initialize the interferometry system, i.e., to get a null field of the image which represents a zero deformation field. The whole optical system was then isolated and kept untouched during the testing procedure. A special high precision device was developed to register the position of the specimen, so that each time the specimen was taken away for thermal cycling, we were able to put it right back at the same position. Another fixture was designed to secure the specimen through the testing and to keep the boundary condition of the specimen unchanged through the entire testing procedure. The technique developed here guaranteed that the temperature gradient was the only loading, and the measured displacement truly represented the irreversible plastic deformation of the specimen.

The specimen was exposed to thermal cycling for certain cycles, then it was taken out to measure the irreversible deformation. It was then put back to the chamber for further cycling. For

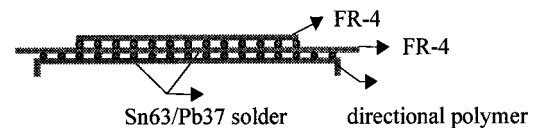


Fig. 10 Cross-section of specimen

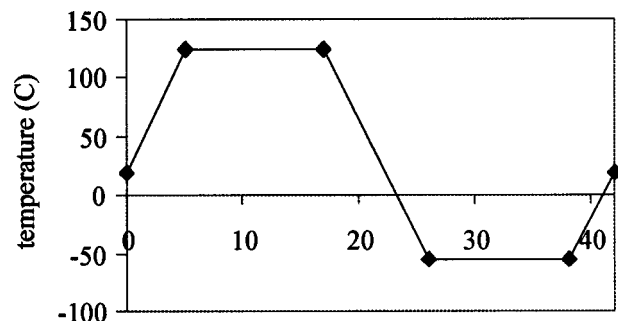


Fig. 11 Temperature history

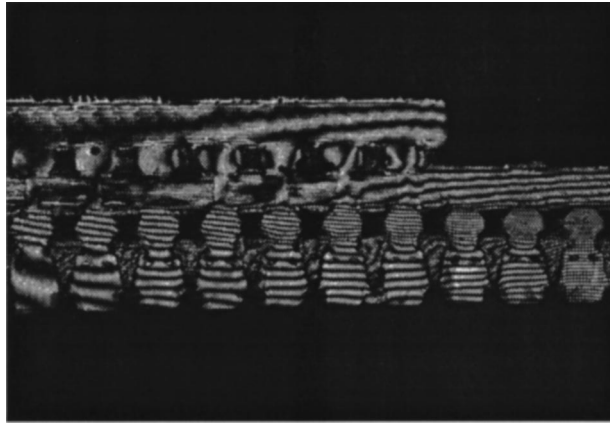


Fig. 12 U fringe field after one thermal cycle

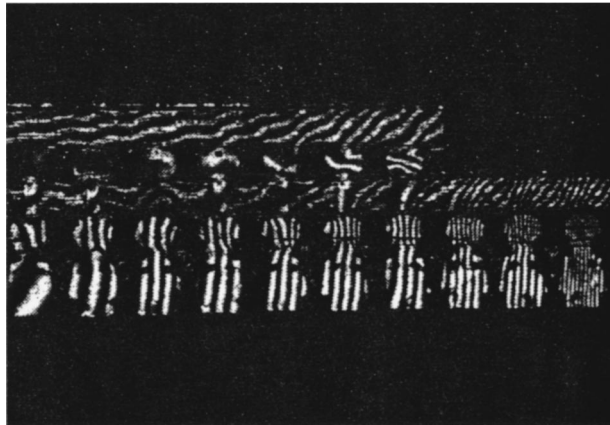


Fig. 13 V fringe field after one thermal cycle

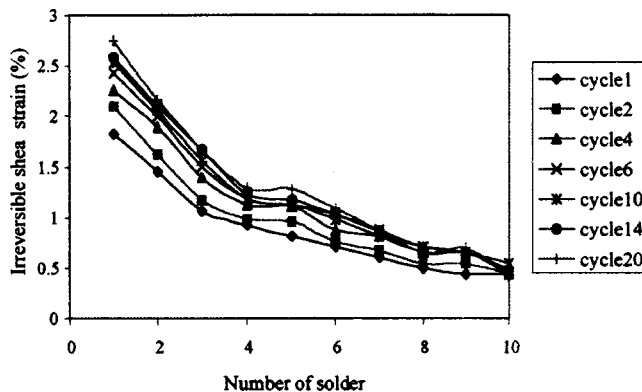


Fig. 14 Irreversible shear strain distribution

each measurement, the total irreversible deformation was recorded and average strain at each solder joint was calculated.

The whole field images of half of the specimen are shown in Fig. 12 and Fig. 13 for the deformation after one cycle. It is also obvious that shear strain gradually increases from the center solder joint (solder 10) to the edge solder joint (solder 1), counting from the free edge to the center. Figure 14 shows the average accumulative irreversible shear strain distribution of the solder joint layer at 1st, 2nd, 4th, 6th, 10th, 14th and 20th cycles. As we can see from Fig. 14 there is no jump near the free edge, the change in strain as we get closer to the edge is gradual. Experimental results indicate that stress distribution obtained in elastic analysis is unrealistic.

Conclusions

Analytical, elastic FEM, viscoplastic, and a damage mechanics based thermo-viscoplastic model are used to study the stress analysis of multilayered structures.

The stress distribution along the interface shows that both shear and peeling effect play important roles in causing the final failure of the structure that is easily to be triggered at the free edge due to the stress concentration.

Suitable mesh refinement has to be satisfied in order to achieve reliable results. Careful selection of material model for the different parts of the structure may reduce the degree of sensitivity, and yield better results with fewer elements.

The elastic FEA analysis is highly mesh sensitive for laminated structures. Hence, using elastic FEA to validate closed-form solutions quantitatively is misleading. The maximum stress levels obtained from viscoplastic model are significantly lower than elastic analysis. Using elastic finite element analysis or elastic closed-form solution to design laminated microelectronics packaging leads to very conservative designs. Therefore, performing inelastic analysis of laminated assembly using damage mechanics based models is essential for final design.

Thermo-viscoplastic with damage analysis results in a more accurate stress diagram along the adhesive layer. In elastic analysis shear and peeling have very high gradients near the free edge at a very narrow region. Qualitative comparison with the experimental results indicate that analysis with viscoplastic damage models yield more realistic results in terms of actual stress distribution profile.

Acknowledgments

This research project is sponsored by the Department of Defense Office of Naval Research PEBB project and NSF/GOALI project CSM Division grant 9908016. Support received from Dr. George Campisi, Program Director at ONR is gratefully acknowledged.

References

- [1] Chen, D., Cheng, S., and Gerhardt, T. D., 1982, "Thermal Stresses in Laminated Beams," *J. Therm. Stresses*, **5**, pp. 67–84.
- [2] Glaser, J. C., 1989, "Thermal Stresses in Compliantly-Joined Materials," ASME Winter Annual Meeting, Paper No. 89-WA/EEP-14, San Francisco, CA, Dec.
- [3] Jiang, Z. Q., Huang, Y., and Chandra, A., 1997, "Thermal Stresses in Layered Electronic Assemblies," *ASME J. Electron. Packag.*, **119**, pp. 127–133.
- [4] Timoshenko, S., 1925, "Analysis of Bi-Metal Thermostats," *J. Opt. Soc. Am.*, **11**, pp. 233–255.
- [5] Boley, B. A., and Testa, R. B., 1969, "Thermal Stresses in Composite Beams," *Int. J. Solids Struct.*, **5**, pp. 1153–1169.
- [6] Wang, S. S., and Crossman, F. W., 1977, "Edge Effects on Thermally Induced Stresses in Composite Laminates," *J. Compos. Mater.*, **11**, pp. 300–312.
- [7] Grimado, P. B., 1978, "Interlaminar Thermoelastic Stresses in Layered Beams," *J. Therm. Stresses*, **1**, pp. 75–86.
- [8] Wang, S. S., and Choi, I., 1979, "Boundary Layer Stresses in Angleply Composite Laminates," *Modern Developments in Composite Materials and Structures*, J. R. Visson, ed., pp. 315–341.
- [9] Chang, F.-V., 1983, "Thermal Contact Stresses of Bi-Metal Strip Thermostat," *Appl. Math. Mech.*, **4**, Tsinghua University, Beijing, China, pp. 363–376.
- [10] Saganuma, K., Okamoto, T., and Koizumi, M., 1984, "Effect of Interlayers in Ceramic-Metal Joints with Thermal Expansion Mismatch," *J. Am. Ceram. Soc.*, **67**, pp. C256–C257.
- [11] Blech, J. J., and Kantor, Y., 1984, "An Edge Problem Having No Singularity at the Corner," *Comput. Struct.*, **18**, pp. 609–617.
- [12] Kuo, A. Y., 1989, "Thermal Stresses at the Edge of a Bimetallic Thermostat," *ASME J. Appl. Mech.*, **56**, pp. 585–589.
- [13] Reddy, J. N., and Miravete, A., 1995, *Practical Analysis of Composite Laminates*, CRC Press, New York.
- [14] Hutchinson, J. W., 1996, *Mechanics of Thin Films and Multilayers*, Solid Mechanics Technical University of Denmark Press.
- [15] Dash, W. C., 1955, *Phys. Rev. A*, **98**, p. 1536.
- [16] Taylor, T. C., and Yuan, F. L., 1962, "Thermal Stress and Fracture in Shear Constrained Semiconductor Device Structures," *International Radio Engineers Trans. on Elect. Dev.*, **ED-9**, pp. 303–308.
- [17] Bogy, D. B., 1968, "Edge-Bonded Dissimilar Orthogonal Elastic Wedges Under Normal and Shear Loadings," *ASME J. Appl. Mech.*, **35**, pp. 460–466.

- [18] Bogy, D. B., 1970, "On the Problem of Edge-Bonded Elastic Quarter-Planes Loaded at the Boundary," *Int. J. Solids Struct.*, **6**, pp. 1287–1313.
- [19] Hein, V. L., and Erdogan, F., 1971, "Stress Singularities in a Two-Material Wedge," *Int. J. Fract. Mech.*, **7**, No. 3, pp. 317–330.
- [20] Zeyfang, R., 1971, "Stresses and Strains in a Plate Bonded to a Substrate: Semiconductor Devices," *Solid-State Electron.*, **14**, pp. 1035–1039.
- [21] Reinhart, F. K., and Logan, R. A., 1973, "Interface Stress of Alx Gal-xAs-GaAs layer structures," *J. Appl. Phys.*, **44**, No. 7, pp. 3171–3175.
- [22] Roll, K., 1976, "Analysis of Stress and Strain Distribution in Thin Films and Substrates," *J. Appl. Phys.*, **47**, No. 7, pp. 3224–3229.
- [23] Olsen, G. H., and Ettenberg, M., 1977, "Calculated Stresses in Multilayered Heteroepitaxial Structures," *J. Appl. Phys.*, **4**, No. 6, pp. 2543–2547.
- [24] Vilms, J., and Kerps, D., 1982, "Simple Stress Formula for Multilayered Thin Films on a Thick Substrate," *J. Appl. Phys.*, **53**, No. 3, pp. 7–13.
- [25] Glascock, H. H., and Webster, H. J., 1984, "Structural Copper: A Pliable High Conductance Material for Bonding to Silican Power Devices," *IEEE Trans. Compon., Hybrids, Manuf. Technol.*, **CHMT-6**, No. 4, pp. 21–28.
- [26] Suhir, E., 1986, "Stresses in Adhesively Bonded Bi-Material Assemblies Used in Electronic Packaging," *Elect. Pack. Mat. Science-II, MRS Symp. Proc.*, pp. 133–138.
- [27] Suhir, E., 1986, "Stresses in Bi-Metal Thermostats," *ASME J. Appl. Mech.*, **53**, No. 3, pp. 657–660.
- [28] Suhir, E., 1986, "Calculated Thermally Induced Stresses in Adhesively Bonded and Soldered Assemblies," *Int. Symp. Microelect.*, pp. 383–392.
- [29] Suhir, E., 1988, "An Approximate Analysis of Stresses in Multilayered Elastic Thin Films," 1988 ASME Winter Annual Meeting, IL, Nov 28–Dec 2, WA/APM-14.
- [30] Suhir, E., 1989, "Interfacial Stresses in Bimetal Thermostats," *ASME J. Appl. Mech.*, **56**, pp. 595–600.
- [31] Suhir, E., 1995, "Global and Local Thermal Mismatch Stresses in an Elongated Bi-Material Assembly Adhesively Bonded at the Ends," *Symp. on Structural Analysis in Microelectronic and Fiber Optic Systems*, 1995 ASME Winter Annual Meeting, EEP/12, pp. 101–105.
- [32] Gerstle, F. P. Jr., and Chambers, R. S., 1987, "Analysis of End Stresses in Glass-Metal Bimaterial Strips," *Technology of Glass, Ceramic, or Ceramic-Glass to Metal Sealing*, Moddeman, W. E., Mertem, C. S., and Kramer, D. P., eds., ASME, MD-Vol. 4, pp. 47–59.
- [33] Yin, W. L., 1991, "Thermal Stresses and Free-Edge Effects in Laminated Beams: A Variational Approach Using Stress Functions," *ASME J. Electron. Packag.*, **113**, pp. 68–75.
- [34] Pao, Y. H., and Eisele, E., 1991, "Interfacial Shear and Peel Stresses in Multilayered Thin Stacks Subjected to Uniform Thermal Loading," *Vol. 113*, pp. 164–172.
- [35] Morgan, H. S., 1991, "Thermal Stresses in Layered Electrical Assemblies Bonded With Solder," *ASME J. Electron. Packag.*, **113**, pp. 350–354.
- [36] Lee, M., and Jasiuk, I., 1991, "Asymptotic Expansions for the Thermal Stresses in Bonded Semi-Infinite Bimaterial Strips," *ASME J. Electron. Packag.*, **113**, pp. 173–177.
- [37] Basaran, C., 1996, "A Comparison of Viscoplastic and Plastic Constitutive Models for Pb/Sn Solder Alloys," *ASME-EEP Structural Analysis in Microelectronics and Fiber Optics*, Vol. 16, pp. 149–154.
- [38] Zhao, Y., Basaran, C., Cartwright, A., and Dishongh, T., 2000, "Thermomechanical Behavior of Microscale Solder Joints," An Experimental Observation, *J. Mech. Behav. Mater.*, **10**, No. 3, pp. 135–146.
- [39] Hacke, P. L., Sprecher, A. F., and Conrad, H., 1997, "Microstructure Coarsening During Thermomechanical Fatigue of Pb/Sn Solder Joints," *J. Electron. Mater.*, **26**, p. 7.
- [40] Kashyap, P., and Murthy, G. S., 1981, "Experimental Constitutive Relations for the High Temperature Deformation of a Pb/Sn Eutectic Alloy," *J. Mater. Sci. Eng.*, **50**, pp. 205–213.
- [41] Basaran, C., and Yan, C., 1998, "A Thermodynamic Framework for Damage Mechanics of Solder Joints," *ASME J. Electron. Packag.*, **120**, pp. 379–384.
- [42] Suhir, E., and Lee, Y. C., 1988, "Thermal, Mechanical and Environmental Durability Design Methodologies," chapter packaging in *Electronic Materials Handbook*, vol 1.
- [43] Suhir, E., 1987, "Stresses in Multilayered Thin Films on a Thick Substrate, Heteroepitaxy-on-Silicon II," *Mater. Res. Soc. Symp. Proc.*, **91**, pp. 73–80.